City Research Online

City, University of London Institutional Repository

Instantaneous and ensemble average cavitation structures in Diesel micro-channel flow orifices

Nicholas Mitroglou[a,*], Michael McLorn[a], Manolis Gavaises[a], Celia Soteriou[b], Mark Winterbourne[b]

[a]*School of Engineering and Mathematical Sciences, City University London, Northampton Square, EC1V 0HB, UK*
[b]*Delphi Diesel Systems, Gillingham, Courteney Rd, ME8 0RU, UK*

Abstract

Cavitation developing upstream and inside the micro-channel orifices of transparent multi-hole fuel injector nozzles has been characterised using a high speed visualisation system. Images have been obtained with short exposure time and sufficiently high spatial and temporal resolution, freezing the formation of cavitation bubbles and their further development during every single injection cycle. Post processing of statistically large number of images collected from many successive injection events and numerous identical nozzles has allowed for the first time estimation of the ensemble average cavitation image and its standard deviation. The instantaneous images reveal the formation of a variety of complex and interacting two-phase flow regimes. Vapour bubbles have been found to exist inside the nozzle prior to start of injection. These bubbles originate from the previous injection cycle as they have not been evacuated from the nozzle and hence, they remain trapped, altering the flow of the subsequent injection event. During the opening and closing stages of the needle valve that controls the fuel flow through the nozzle, cavitation is found to form in the valve's seat area. Subsequently, vortex or 'string' cavitation has been recorded to take place in a rather chaotic manner; its life time and most probable location of appearance have been estimated. The ensemble average images reveal the probability of cavitation appearance at a specific location within the nozzle and the micro-channel flow orifice. The standard deviation from the mean reveals locations with significant cycle-to-cycle variations of the flow. These are linked to significant deviations from the mean of the fuel spray dispersion angle forming downstream of the nozzle exit.

Keywords: Two-phase flow, cavitation, Diesel fuel injection, realistic nozzle tip design

1. Introduction

Cavitation is known to form inside various injector nozzle designs featuring micro-hole channels [1, 2, 3]; it is the dominant but largely uncontrolled flow characteristic causing surface erosion. It is also believed to improve the atomisation of the spray plume downstream of the nozzle exit. Despite its significance, the details of cavitation formation in such flow orifices still

---

remain unclear. This can be mainly attributed to the difficulty in manufacturing transparent nozzle replicas at 1:1 scale, as the nozzle orifice diameter is of the order of 10^{-4} m, the extremely high operating pressure that varies between 100 to 3000 bar and the very short time scales of the injection event, which typically last around 1ms. Enlarged nozzle replicas have provided insight on cavitation structures, as demonstrated in [4, 5]; typically, two distinct macroscopic forms of cavitation have been identified, which have been referred to as geometrically-induced and vortex or 'string' cavitation. The former is the most common form of cavitation in such flow orifices and it has become gradually a relatively well-understood phenomenon; appropriate design of the inlet hole curvature and non-cylindrical injection hole shapes (often referred to as *tapered*) alter cavitation inception, as shown in [6, 7]. On the other hand, vortex cavitation is believed to represent a flow feature that depends mainly on the development of turbulent flow within the nozzle rather than a phenomenon that can be controlled by the nozzle design, as it is the case with the geometric-induced cavitation [see 8, 9]. Vortex cavitation is commonly found in propellers, hydraulic turbines and hydrofoils as explained in [10, 11, 12, 13]; further studies have also confirmed similar structures in a variety of nozzle designs [14, 15] and even at pressures as high as 2000 bar, as shown in [16].

The majority of transparent real-size nozzles feature simplified single-hole geometries that generally confirm the presence of geometric-induced cavitation [17, 18, 19, 20, 2]. The work of [3] and their follow-up of [21, 22] were the first to substitute one of the holes of a production nozzle with a quartz window of identical geometric characteristics and was an experimental breakthrough that provided valuable information on flow and cavitation structures inside such micro-channels under realistic operating conditions. A step forward was realised in [23], where a 3-hole, real-size, fully transparent nozzle allowed for unobstructed optical access inside the sac volume. In [5] there is evidence that geometric-induced and vortex cavitation are interrelated. String cavitation is dramatically enhanced and owes its existence to sources of vapour already present inside the nozzle volume [8]. Moreover, [24] showed that the structure of a vortex core is significantly affected by entrained vapour bubbles. Similarly, [25] demonstrated possible fragmentation of the vortex core so as to increase the vorticity at the core centre. Finally, the strong interaction observed between vortex properties and bubble dynamics [26], the coupling of radial and axial growth of bubbles trapped in vortices [27] and the interaction between shear (or normal strain) flow and bubble volume change [28] form a tremendously complex flow field inside an injector nozzle, where dynamic changes in the behaviour of vortices and vapour bubbles strongly affect the emerging fuel spray. Highly transient flow phenomena caused by the fast needle response times, give rise to formation of vortical structures and therefore, to string cavitation [8]. Transient effects have also been correlated to increased probability of surface erosion damage, which is attributed to both, geometric and string cavitation [29]. Unfortunately, all relevant studies so far report data from one or just a few injection events. No effort has been made to characterise the cavitating flow over a sufficient large number of injection events that would allow for a thorough description of the relevant phenomena.

The present contribution relates instantaneous and mean cavitation structures developing inside real-size fully transparent nozzle replicas; these replicas offered unobstructed simultaneous optical access of the nozzle's sac volume, the micro-channel flow orifices and the fuel spray plumes forming downstream of the nozzle exit. High speed visualisation featuring short enough exposure times and adequate spatial and temporal resolution enabled the recording of cavitation initiation and further development. Images have been obtained from a large number of injection events and numerous identical nozzle tips resulting in a statistically large sample. Their post processing has allowed for estimation of the ensemble average cavitation image and its standard
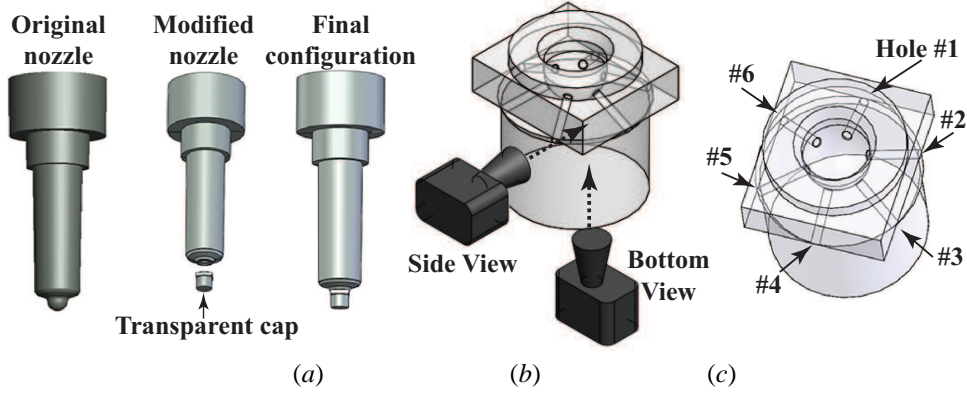
Figure 1: (*a*) Manufacturing steps of transparent nozzle tip assembly [31],(*b*) side view of transparent nozzle tip indicating the side and bottom views and (*c*) 3-D view of transparent tip indicating the hole numbering.

deviation to be derived for the first time in the relevant literature for a real high-pressure Diesel nozzle geometry. Such data not only reveal new aspects of the relevant phenomena, but they can be valuable for thorough validation of relevant LES or ensemble averaged (RANS) CFD models. Past relevant studies [30] had focused on and presented steady-state averaged cavitation images and velocity profiles of flow through a single-hole plate orifice. The next section describes the experimental method and data analysis employed, followed by the presentation of the results; the most important conclusions are summarised at the end.

2. Experimental set up and technique

The details of the experimental test rig and injector set up utilised in the present study are described thoroughly in [31] while a schematic of the modified nozzle employed here is illustrated in figure 1(*a*). As the structural strength of Perspex in compression is limited, a suitable force able of providing sealing to fuel pressures up to 500 bar has been utilised; unfortunately, this prevented experiments to be performed at higher pressures. The prototype nozzle geometry chosen has six cylindrical orifices attached to the nozzle's sac volume; such nozzle designs are typically utilised with Diesel injectors (figure 1). The injection hole diameter is 0.160 mm ±2%, a value not far from the manufacturing tolerances of metallic nozzles. The initial design involved only parallel injection holes symmetrically positioned at an angle of 65 ° to the injector's axis of symmetry. The transparent nozzle tips feature hole inlet rounding which was achieved using the extrude hone process realised by an abrasive flow machine (AFM). This results to non-uniform hole inlet rounding that exhibits larger radius of curvature at the top-side hole inlet compared to the bottom-side hole inlet; indicative radius of curvature achieved are of the order of 0.01 mm ±0.003 mm, for the bottom side inlet and 0.025 mm ±0.005 mm, for the top side inlet.

The best-suited imaging technique for visualisation of internal nozzle cavitation structures at such scale was identified to be a combination of shadowgraphy and Mie scattering. The experimental arrangement involves two high-speed cameras, utilising side and bottom views, focused on the injection hole and the sac volume of the transparent tip, respectively. The side-view camera captures shadows of cavitation structures inside the injection hole and the emerging spray plume, simultaneously. The second camera utilises light reflections from the interface between

cavitation vapour clouds and the surrounding liquid inside the nozzle's sac volume. The lenses set up ensures a square pixel shape of 3.4×10^{-3} mm edge size that results in a 1.752 mm^2 imaging area, given the camera resolution is set to 592×256 pixels at frame rates of 30 000 and 50 000 frames per second; the selected frame rates resolve a typical injection event lasting for 2ms with 60 to 100 images, respectively. The high magnification achieved for the side view images permitted the tracing and extraction of the needle valve motion. Additionally, a common rail pressure sensor and an in-line pressure transducer installed upstream the injector fuel inlet provided detailed time-resolved pressure fluctuations. For the present investigation, an injection pressure of 300 bar was chosen and single injection strategy of 2 ms electronic pulse duration; injection takes place under atmospheric pressure and room temperature. As transparent nozzles made from Perspex fail (deform or even break) after a relatively small number of injections, a large number of nozzle tips had to be manufactured. A series of tests have shown that at injection pressures of around 400 bar, internal geometry deterioration was profound after 160-180 injection events. Following inspection of a large number of nozzles at successive injections through silicon prints and the subsequent 3-D reconstruction of the nozzle's geometry variation, it was established that a safe threshold above which a tip was considered "used" was 50 injections. In order to avoid overheating of the Perspex nozzle tip, the nozzle was left to rest after 10 successive injection events. In total, 250 nozzle tips have been utilised, resulting in acquisition of more than 12 500 images for each of the 100 time instances resolving transiently the injection event.

The acquired side and bottom view images have been processed accordingly in order to provide information in terms of needle valve lift, sac flow conditions prior to start of injection, cavitation development and emerging spray stability. As mentioned, continuous wide band light sources have been used along with a series of focusing lenses to concentrate available light intensity on to the investigated nozzle tip. Following thresholding and binarisation of each of the acquired images, the ensemble average image and the corresponding standard deviation were calculated at given time instances over all acquired injection events and for all transparent nozzle tips, applying equations 1a,b; where I represents a single pixel intensity value, $\bar{I}$ represents mean pixel intensity value and N is the number of samples. A robust post-processing procedure was secured by an automated selection of the binarisation threshold that was based on a 2-dimensional histogram approach found in [32]; this method is an extension of the well-known threshold selection method from grey-level histograms of Otsu, [33]. Given the applied post-processing method and the number of samples used, the calculated statistical uncertainty is 0.2%. Cavitation structures inside a real-size nozzle are known to exhibit highly transient behaviour thus, standard deviation images proved to be very informative, in terms of location of unstable cavitation structures. It should be noted that the present analysis only provides the projection of cavitation cloud on the imaged 2-D plane, and thus, information related to the three dimensional structure of cavitation along the depth of the orifices cannot be resolved. Finally, bottom view images have been analysed for identification of string cavitation presence and location inside the sac volume of the nozzle.

$$\bar{I} = \frac{\sum_{i=1}^{N} I}{N}, \quad \sigma_I = \sqrt{\frac{1}{N} \sum_{i=1}^{N}(I - \bar{I})^2} \qquad (1a, b)$$

Furthermore, the presented average fuel injection rate was measured by an IAV Injection Analyser that utilises the Bosch operating principle. The accuracy of the measurements, as specified by the manufacturer, was ±0.6 mg/stroke for the measured quantities. Finally, the working fluid for the present study was chosen to be European Diesel oil type A that is found widely in the
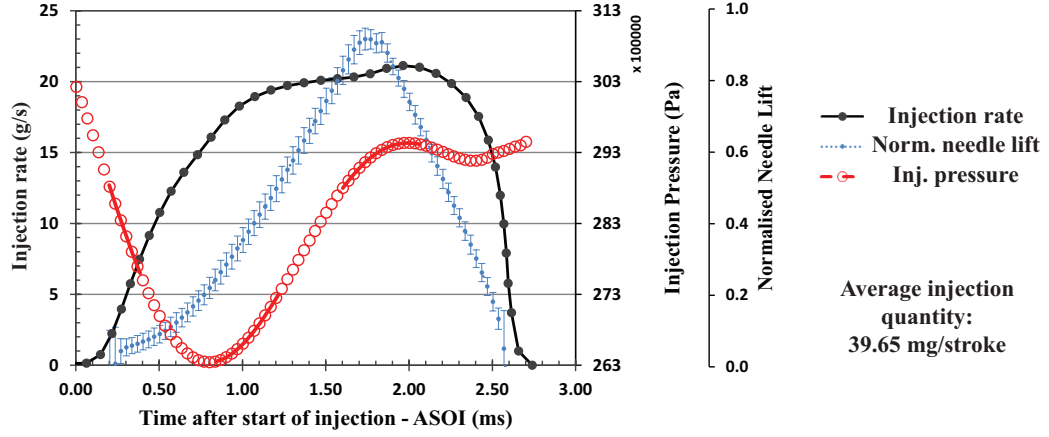
Figure 2: Mean curves of injection rate, needle valve lift and injector line pressure for injection duration of 2 ms at 300 bar injection pressure.

market. The properties of the working fluid follow the EN 593 standard and are summarised as follows: density of 830 kg/m^3, viscosity of 3×10^{-6} m^2/s and vapour pressure of 1-10 kPa, all at 40°C; additionally, the typical flash point of Diesel oil type A is set at 50°C.

3. Results and discussion

In this section, the results obtained are described. Initially, we report data referring to inlet pressure, flow rate and needle lift measurements. Then a description of the flow processes is attempted by analysing the images obtained from a representative injection cycle. Finally, the statistical description of the flow is presented.

3.1. Needle lift and pressure

The nozzle's volumetric capacity characterisation was carried out for a number of transparent tips. The mean injection rate curve is illustrated in figure 2, along with data acquired from the installed pressure transducers and the needle valve lift as extracted from the acquired images. The mean injected quantity was measured to be 39.65 mg/stroke. As illustrated in figure 2, fuel injection rate increases slowly for the first millisecond, being in full agreement to the needle lift curve that exhibits a relatively slow opening response during the same time; the latter was expected due to the low injection pressure setting. At the same time, mean injection pressure levels at the injector fuel entry feature a drop of approximately 40 bar, before recovering almost 3/4 of this drop in the following 1 ms. At the elapse of this time, needle valve lift has almost reached its maximum position (~0.92 of nominal full lift). The standard deviation over all injection events was estimated for the needle lift and pressure traces (figure 2). Maximum values do not exceed ±3.5%, for the needle lift trace during the time the needle has lifted more than 20% of its nominal full lift, and 3% for the pressure traces; the latter, gives confidence that inlet fuel pressure and needle valve motion were repeatable throughout the thousands of injections recorded.

3.2. Representative flow images

We now turn to the analysis of the cavitation images obtained. Initially, a representative injection event is presented, as this reveals the various mechanisms of cavitation inception and development. The first important observation was made before the needle valve energisation and reveals that prior to start of injection the nozzle's sac volume is partially occupied by bubbles rather than liquid, as perceived up to now. The bubble pattern does not appear to be repeatable; it may consist of either single large diameter bubbles or smaller multiple bubbles. At the same time, the micro-channels appeared to be partially filled with stagnant vapour as depicted in figure 3. These cavitation bubbles are created at the needle seat area during the latest stages of the valve closing phase. They do not exit the nozzle and therefore reside inside the sac volume forming the observed fuel liquid/vapour mixture; these bubbles rest in the nozzle between successive injection events without much activity. However, it has been observed that given sufficient time, these bubbles may coalesce to form larger ones or even a single bubble that can occupy most of the nozzle's sac volume. Interestingly enough, ambient air entering into the nozzle through the injection holes has been also identified. The latter phenomenon has been observed consistently following the closure of the needle valve.

Cavitation forming in the needle seat area, is also pronounced during the opening stages of the needle valve. In figure 3, and at 0.04 ms and 0.07 ms, images acquired during a single injection event illustrate the appearance of cavitation bubbles entering the sac volume, as needle valve starts lifting. These cavitation bubble clouds seem to gradually disintegrate to much finer structures as the pressure inside the nozzle's sac volume rises until reaching eventually the inlet of the orifices; there they either re-grow forming a larger volume cavitation cloud or induce formation of cavitation near the inlet walls of the micro-channel orifices. The latter phenomena has been reported in [8] but under fixed needle lift conditions. As needle valve continues to lift, cavitation ceases formation in this area and the fresh fuel entering into the sac volume pushes the remaining bubbles towards the injection holes. Following this time, the appearance of string cavitation becomes evident at time instances between 0.66 ms and 0.85 ms as illustrated in figure 3. String cavitation formation seems to be triggered by micro-bubbles entering into the injection holes, trapped into regions of relatively low pressure (recirculation zones) and taking finally the elongated observed vapour tube shape. As needle valve continues to lift to about 20% of its nominal maximum level, the observed string cavitation structures inside the injection holes develop in a much more aggressive manner. String cavitation is observed to extend from one injection hole to another, resulting in hole inter-connecting vapour tubes, or in hole to needle tip strings. The highly transient nature of these structures is reflected on their residence time-scales inside the sac volume. In the case of 30 000 frames per second, almost 20% of the recorded cavitation strings lived for just one frame; however, this percentage dropped to 8%, when image acquisition frequency was increased to 50 000 frames per second, which implies that the temporal resolution of the high speed camera can be limiting our measurements in capturing even faster processes. On the other hand, the maximum recorded string residence time has been observed to rise to values as high as 0.3 ms, which represents about 1/3 of a nominal injection event. Nevertheless, cavitation strings appearing at time scales shorter than those captured by the frame rates available cannot be excluded. This limitation, arising from the hardware used, could have an impact on the plotted results. However, strings with appearance of only one frame currently represent less than 8% for the highest image acquisition frequency used (50kHz). As needle valve lifts beyond 40% of its maximum lift little cavitation activity is observed in the nozzle's sac volume; cavitation strings are now confined inside the injection holes co-existing and interacting with geometric cavitation. The later firstly appears at the bottom side of the injection hole and it is
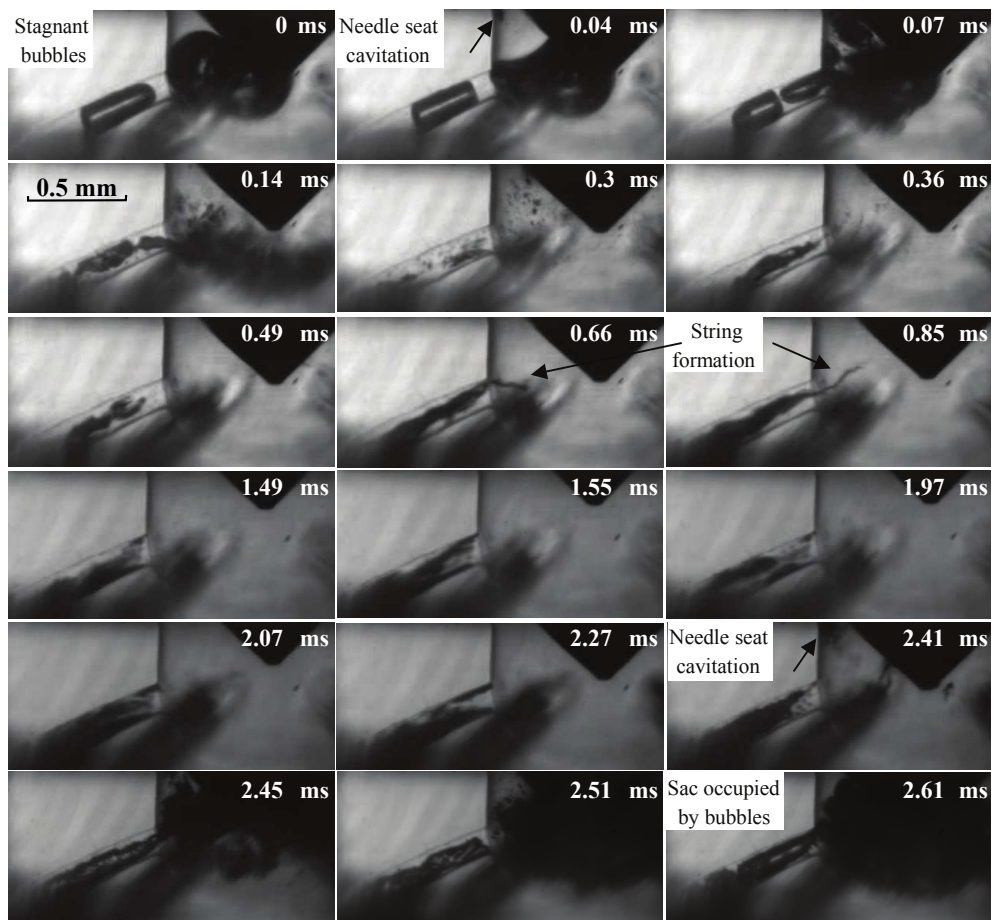
6

Figure 3: Sequence of representative side view high-speed images at selected time instances after start of injection single injection event of 2 ms duration at 300 bar injection pressure.

visible for the whole injection duration. The fact that the hole inlet features a radius of curvature which is larger at the upper part does not favour formation of geometric cavitation at that location. Cavitation strings appear mainly on the upper part of the hole which is mainly occupied by liquid; this can be seen at 1.49 ms on the images of figure 3. However, their appearance seems to become visible only sporadically throughout the injection event. A statistical description of their appearance is given in the following section. Finally, towards the end of injection, the flow presents some similarities to the needle opening phase. Still, appearance of cavitation strings seem to be less frequent, which implies that as the flow becomes well developed and organised during the main part of injection, smaller scale and randomly appearing vortices are less probable to form. Finally, as mentioned earlier, needle seat cavitation appears at the latest stages of the needle closing phase, feeding bubbles into the sac volume which can be seen at the start of a consequent injection event.

3.3. Statistical description

We now turn to the presentation of the statistical description of the acquired images. This can be divided into two sub-sections: *(i)* life time and location of appearance of cavitation strings within the sac volume and *(ii)* mean and standard deviation cavitation images within the injection hole and the near nozzle spray plume formation.

As mentioned in the previous section, the location and life time of individual cavitation strings seem to vary considerably. As detailed 3-D coordinate information related to the area of their formation was not possible, their location of appearance has been correlated with the hole numbering of figure 1; this is indicated on the *Y*-axis in figure 4. The *X*-axis corresponds to time, resolving a full injection event. The plot represents the frequency of appearance of a string attached to a particular micro-channel and it has been derived by considering all acquired images from all nozzle tips manufactured. During the initial stages of the injection event, formation of strings seems to be much more pronounced; peak values of 20% indicate that a string is attached to a particular injection hole almost 1/5 of the total running time. However, once the needle valve reaches its maximum lift, the appearance of strings becomes far less frequent. The corresponding values now drop down to less than 5% and remain at this level until the end of injection. It is also noticeable that 3 out of the 6 micro-channels exhibit lower levels compared to the other three; this can be interpreted as an indication of flow asymmetries that can be attributed to eccentric needle valve opening as well as its possible rotation which can be speculated from its design. The data described above can be used to validate corresponding LES models predicting the frequency of formation of vortical structures in such geometries.

We now turn to the description of the ensemble averaged flow images inside the micro-orifices. Figure 5 presents mean images and the corresponding standard deviation at selected time instances during an injection event; images below 1.5 ms after start of injection correspond to the opening phase of the needle valve, time steps between 1.5 - 2 ms represent mid-injection stroke and needle valve lifts larger than 80%, while remaining images above 2 ms correspond to the valve closing event. The images reveal that the lower part of the injection hole is always occupied by cavitation, and thus mean values approach 100%. On the contrary, the upper part seems much less influenced by cavitation in a rather unstable mode. Cavitation is present in such location for no more than 50% of the running time; consequently, the highest values of standard deviation can be observed. The large values of standard deviation observed on the upper part of the orifices can be related to spray angle, which has been imaged simultaneously with the nozzle flow. Inspection of images shows that the upper part of the injected spray plume also exhibits a fluctuating behaviour. At the start of injection, when the velocity is relatively low,
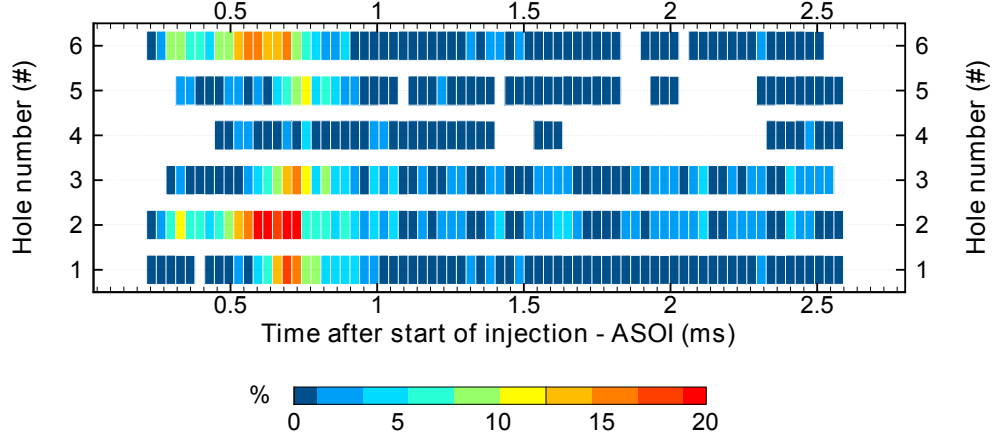
8

Figure 4: Ensemble average cavitation string appearance adjacent to an injection hole during the injection event; averages have been obtained from the acquired bottom view images of all injection cycles and nozzle tips tested.

a non-repeatable spray pattern forms from injection to injection at the nozzle exit. As velocity increases (figure 5 @ time steps larger than 0.7 ms), this fluctuating behaviour seems to appear further downstream of the nozzle exit. Finally, at time steps later than 2.25 ms after start of injection and as needle valve lift drops at values below 80%, the observed emerging spray exhibits significant cycle-to-cycle fluctuations, as illustrated in the standard deviation images of figure 5. From the inspection of the instantaneous raw images inside an injection hole, it has been found that cavitation strings change their location on average every 0.033 ms and this was reflected in the injected spray plume; the corresponding change to the spray angle was measured to be as high as 35 ° on the upper spray boundary, and almost 5 ° on the lower spray boundary (figure 5). Such behaviour is in accordance with the observations in [34], where similar values have been reported but for different types of enlarged nozzle models operating under lower pressures and fixed needle lift conditions.

4. Conclusions

High-speed images of cavitation structures forming inside real-size, transparent nozzles featuring cylindrical micro-hole flow channels attached to a sac volume have been obtained. In addition to the instantaneous cavitation images, recording of sufficient large number of injection cycles has allowed for the first time a statistical description of the significant cycle-to-cycle variations of the flow developing within the nozzle's sac volume, the micro-channel orifices and their influence on the fuel spray dispersion angle forming downstream of the nozzle exit. This has been made possible by manufacturing a large number of transparent nozzle tips while each injection event has been resolved with high temporal and spatial resolution. The results reveal flow regimes not known from previous relevant studies. In particular, the presence of vapour bubbles inside the nozzle prior to start of injection has been identified. These bubbles originate from previous injection cycles as they have not been evacuated from the sac volume and hence, they remain trapped and alter the flow field of the subsequent injection event. Upon start of injection, cavitation is found to form in the needle seat area. Although the well known cavitation
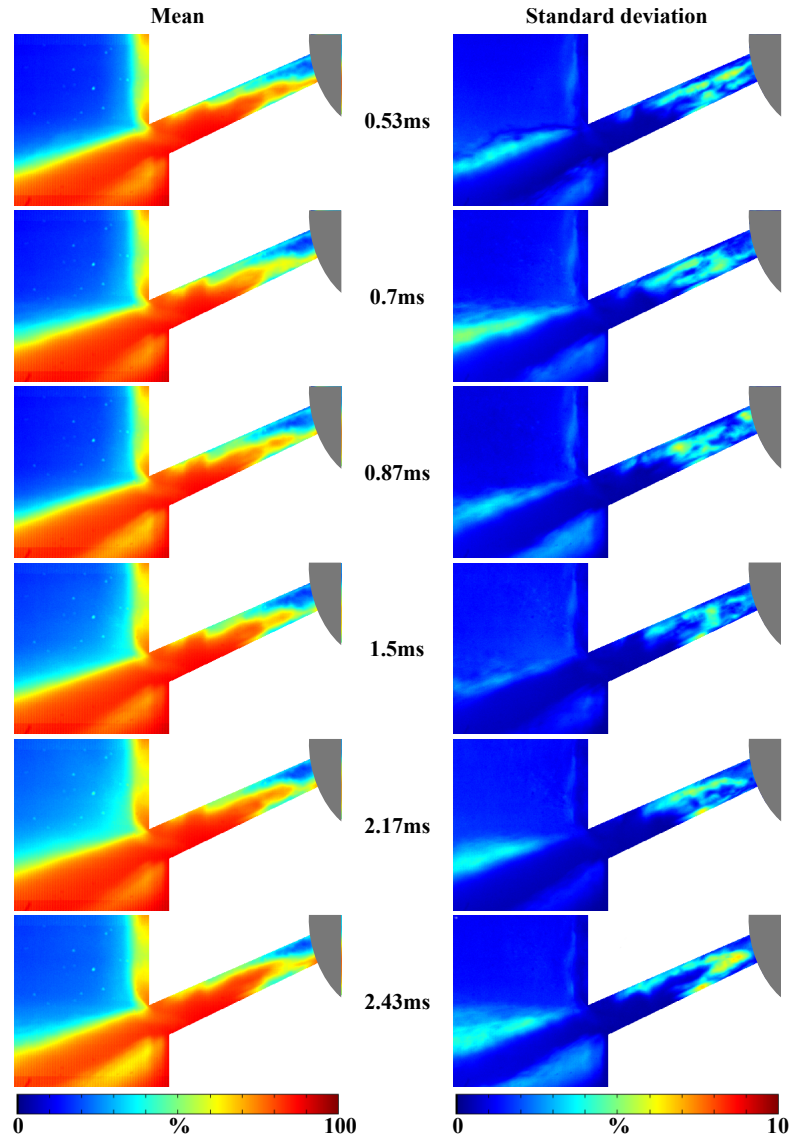
Figure 5: Spatial distribution of ensemble average and standard deviation of cavitation (inside the nozzle) and liquid fuel (downstream of the nozzle exit) presence during selected time-steps of one injection event; averages have been obtained from the side view images of all acquired injection cycles and nozzle tips tested.

erosion in such areas manifests the existence of cavitation, direct visualisation in this location in real-size injectors has not been reported previously. Needle seat cavitation feeds bubbles to the nozzle's sac volume, which act as the necessary traces for the formation of the observed cavitation 'strings'. The latter have been recorded to take place mainly during the opening phase of the needle valve. Their frequency of appearance and life time have been estimated and linked to the instabilities observed on the angle of the fuel spray plume emerging from the nozzle, which has been visualised simultaneously with the cavitating flow inside the micro-channel orifices. Post processing of the images obtained over a large number of injection events and from all transparent nozzles tested has provided, in addition to the instantaneous flow structures, the ensemble average cavitation presence and its standard deviation on the projected 2-D plane imaged, transiently resolved during the injection event. Finally, the present study has provided a number of experimental data covering flow investigations during a complete injection event at realistic injection pressures focused on both, internal nozzle flow and its immediate effect on spray instabilities that are expected to contribute towards future Diesel nozzle design improvements and their consequent computational fluid dynamics studies by providing realistic initial conditions.

5. Acknowledgements

References

[1] H. Chaves, M. Knapp, A. Kubitzek, F. Obermeier, Experimental study of cavitation in the nozzle hole of diesel injectors using transparent nozzles, SAE Technical Paper 950290.

[2] C. Badock, R. Wirth, A. Fath, A. Leipertz, Investigation of cavitation in real size diesel injection nozzles, International journal of heat and fluid flow 20 (5) (1999) 538–544.

[3] C. Arcoumanis, M. Badami, H. Flora, M. Gavaises, Cavitation in real size multi-hole diesel injector nozzles, SAE Technical Paper 2000-01-1249.

[4] C. Arcoumanis, M. Gavaises, J. M. Nouri, E. Abdul-Wahab, R. Horrocks, Analysis of the flow in the nozzle of a vertical multi-hole diesel engine injector, SAE Technical Paper 980811.

[5] H. Roth, M. Gavaises, C. Arcoumanis, Cavitation initiation, its development and link with flow turbulence in diesel injector nozzles, SAE Technical Paper 2002-01-0214.

[6] M. Blessing, G. Konig, C. Kruger, U. Michels, V. Schwarz, Analysis of flow and cavitation phenomena in diesel injection nozzles and its effects on spray and mixture formation, SAE Technical Paper 2003-01-1358.

[7] C. Soteriou, M. Lambert, S. Zuelch, D. Passerel, The flow characteristics of high efficiency diesel nozzles with enhanced geometry holes, in: International Conference on Thermo- and Fluid Dynamic Processes in Diesel Engines, 2006.

[8] A. Andriotis, M. Gavaises, C. Arcoumanis, Vortex flow and cavitation in diesel injector nozzles, Journal of Fluid Mechanics 10 (2008) 195–215.

[9] M. Gavaises, A. Andriotis, D. Papoulias, N. Mitroglou, A. Theodorakakos, Characterization of string cavitation in large-scale diesel nozzles with tapered holes, Physics of Fluids 21 (2009) 052107.

[10] R. E. A. Arndt, Cavitation in fluid machinery and hydraulic structures, Annual Review of Fluid Mechanics 13 (1) (1981) 273–326.

[11] C. T. Hsiao, L. L. Pauley, Numerical study of the steady-state tip vortex flow over a finite-span hydrofoil, Journal of Fluids Engineering 120 (1998) 345.

[12] R. E. A. Arndt, Cavitation in vortical flows, Annual Review of Fluid Mechanics 34 (1) (2002) 143–175.

[13] C. T. Hsiao, G. L. Chahine, Numerical study of cavitation inception due to vortex/vortex interaction in a ducted propulsor, Journal of Ship Research 52 (2) (2008) 114–123.

[14] M. Gavaises, Flow in valve covered orifice nozzles with cylindrical and tapered holes and link to cavitation erosion and engine exhaust emissions, Int. J. of Engine Research 9 (6) (2008) 435–447.

[15] J. M. Nouri, N. Mitroglou, Y. Yan, C. Arcoumanis, Internal flow and cavitation in a multi-hole injector for gasoline direct-injection engines, SAE Technical Paper 2007-01-1405.

[16] B. A. Reid, G. K. Hargrave, C. P. Garner, G. Wigley, An investigation of string cavitation in a true-scale fuel injector flow geometry at high pressure, Physics of Fluids 22 (3) (2010) 031703.

[17] H. K. Suh, C. S. Lee, Effect of cavitation in nozzle orifice on the diesel fuel atomization characteristics, International Journal of Heat and Fluid Flow 29 (4) (2008) 1001–1009.

[18] R. Miranda, H. Chaves, U. Martin, F. Obermeier, Cavitation in a transparent real size vco injection nozzle, in: 9th International Conference on Liquid Atomisation and Spray Systems, 2003.

[19] I. Gilles-Birth, M. Rechs, U. Spicher, S. Bernhardt, Experimental investigation of the in-nozzle flow of valve covered orifice nozzles for gasoline direct injection, in: Proceedings of the 7th International Symposium on Internal Combustion Diagnostics, 2006, pp. 59–78.

[20] R. Payri, F. J. Salvador, J. Gimeno, O. Venegas, Study of cavitation phenomenon using different fuels in a transparent nozzle by hydraulic characterization and visualization, Experimental Thermal and Fluid Science 44 (0) (2013) 235–244.

[21] C. Arcoumanis, M. Gavaises, H. Flora, H. Roth, Visualisation of cavitation in diesel engine injectors, Mec.Ind. 2 (2001) 375–381.

[22] H. Roth, E. Giannadakis, M. Gavaises, C. Arcoumanis, K. Omae, I. Sakata, M. Nakamura, H. Yanagihara, Effect of multi-injection strategy on cavitation development in diesel injector nozzle holes, SAE Technical Paper 2005-01-1237.

[23] H. Chaves, R. Miranda, R. Knake, Particle image velocimetry measurements of the cavitating flow in a real size transparent vco nozzle, in: 22nd European Conference on Liquid Atomization and Spray Systems, 2008.

[24] G. Sridhar, J. Katz, Effect of entrained bubbles on the structure of vortex rings, Journal of Fluid Mechanics 397 (1999) 171–202.

[25] A. J. Cihonski, J. R. Finn, S. V. Apte, Volume displacement effects during bubble entrainment in a travelling vortex ring, Journal of Fluid Mechanics 721 (2013) 225–267.

[26] J. Choi, S. L. Ceccio, Dynamics and noise emission of vortex cavitation bubbles, Journal of Fluid Mechanics 575 (2007) 1–26.

[27] J. Choi, C.-T. Hsiao, G. Chahine, S. Ceccio, Growth, oscillation and collapse of vortex cavitation bubbles, Journal of Fluid Mechanics 624 (2009) 255–279.

[28] S. Dabiri, W. A. Sirignano, D. D. Joseph, Interaction between a cavitation bubble and shear flow, Journal of Fluid Mechanics 651 (2010) 93–116.

[29] M. Gavaises, D. Papoulias, A. Andriotis, E. Giannadakis, A. Theodorakakos, Link between cavitation development and erosion damage in diesel injector nozzles, SAE Technical Paper 2007-01-0246.

[30] E. Winklhofer, E. Kull, E. Kelz, A. Morozov, Comprehensive hydraulic and flow field documentation in model throttle experiments under cavitation conditions, in: Proceedings of the ILASS-Europe Conference, Zurich, 2001, pp. 574–579.

[31] L. Liverani, C. Arcoumanis, H. Yanagihara, I. Sakata, K. Omae, Imaging of the flow and cavitation formation in a transparent real-size six-hole nozzle under realistic conditions, in: 7th International Conference on Modeling and Diagnostics for Advanced Engine Systems, 2008.

[32] L. Jianzhuang, L. Wenqing, T. Yupeng, Automatic thresholding of gray-level pictures using two-dimension otsu method, in: Proceedings of the Circuits and Systems Conference, China., Vol. 1, 1991, pp. 325–327.

[33] N. Otsu, A threshold selection method from gray-level histograms, Automatica 11 (285-296) (1975) 23–27.

[34] A. Andriotis, M. Gavaises, Influence of vortex flow and cavitation on near-nozzle diesel spray dispersion angle, Atomization and Sprays 19 (3) (2009) 247–261.